ADVANCED MATERIALS TECHNOLOGIES
www.advmattechnol.de

3D Printing of Core–Shell Capsule Composites for Post-Reactive and Damage Sensing Applications

*Harald Rupp and Wolfgang H. Binder**

3D printing of multicomponent materials as an advantageous method over traditional mold casting methods is demonstrated, developing small core–shell capsule composites fabricated by a two-step 3D printing process. Using a two-print-head system (fused deposition modeling extruder and a liquid inkjet print head), micro-sized capsules are manufactured in sizes ranging from 100 to 800 μm. The thermoplastic polymer poly(ε-caprolactone) (PCL) is chosen as matrix/shell material due to its optimal interaction with the embedded hydrophobic liquids. First, the core–shell capsules are printed with model liquids and pure PCL to optimize the printing parameters and to ensure fully enclosed capsules inside the polymer. As a proof of concept, novel "click" reaction systems, used in self-healing and stress-detection applications, are manufactured in which PCL composites with nano- and micro-fillers are combined with reactive, encapsulated liquids. The so generated 3D printed core–shell capsule composite can be used for post-printing reactions and damage sensing when combined with a fluorogenic dye.

1. Introduction

Besides stereolithography or selective laser sintering, fused deposition modeling technology (FDM) is one of the most used 3D printing techniques.[1] FDM is highly successful in printing pure polymer materials (like acrylonitrile/butadiene/styrene-copolymer (ABS), polylactic acid (PLA), Nylon, polycaprolactone (PCL)), extruding the thermoplastic polymers in a "never ending" strand, limited only by the polymers melt viscosity to ensure homogeneous extrusion and self-supporting strength after printing.[1b] The properties of the 3D printed objects can be well controlled by layer thickness, orientation, grid width, and angle.[2] Structural components different from the extruded polymer are conventionally introduced directly as a mixture within the extruded polymer via the incorporation of particles, fibers, or nanoparticles to improve structural stability. In particular by use of photopolymerization a large plethora of different and highly complex structures have been addressed such as the 3D printing of compositional gradients for microfluidics,[3] 3D printing of ionogels for stretchable sensors,[4] shape-deformable hydrogels,[5] or specific methodological developments such as the removal of overhanging structures without the need for supportive materials.[6] There is also ample application of 3D printing in the areas of energy materials (thin film solar cell technology, super capacitors, multilayered systems), where many different components (solids and liquids) are required to be printed into one and the same material.[7] Modern FDM printers offer further flexibility in material design when combined with additional printing or dispensing heads, enabling to generate multicomponent materials.[8] If the second printing head is designed as a liquid dispensing unit, the dual printing head 3D printer can be used to create more sophisticated structures, of such a embedded liquids in solid samples or even capsule-like structures, in this way strongly facilitating the need for adjustment of ink-composition, as by separate use of the dispensing systems, only the rheological properties of the native inks need to be considered. Thus, 3D printing can generate liquid core–shell capsules by interrupting the printing of the shell, subsequently filling the core and then again finishing the printing process.[9] Other approaches of embedding liquid-filled capsules via FDM-methods relied on the separate printing of two capsule halves, subsequently filled after printing and subsequent connection of both.[10] Large liquid-filled capsules (core sizes 4–7 mm) were 3D printed using FDM for the capsule shell, simultaneously dispensing a solution of a drug into the capsule.[11] Further approaches towards 3D printed capsules (mm sized) have been published;[12] however, the printing of small (μm sized) capsules is far less known using FDM printing, as processing of very small structures in 3D printing with FDM and dispensing technologies are difficult.[13] Successful methods were published based on hydrogels selectively filled with inkjet printing,[14] presenting a method to 3D-print core–shell capsules within hydrogel matrices. These 3D-printing-based methods included capsule suspensions (200 μm), precise patterning of capsule

H. Rupp, Prof. W. H. Binder
Macromolecular Chemistry
Division of Technical and Macromolecular Chemistry
Institute of Chemistry
Faculty of Natural Sciences II (Chemistry, Physics and Mathematics)
Martin Luther University Halle-Wittenberg
von-Danckelmann-Platz 4, Halle D-06120, Germany
E-mail: wolfgang.binder@chemie.uni-halle.de

The ORCID identification number(s) for the author(s) of this article can be found under https://doi.org/10.1002/admt.202000509.

DOI: 10.1002/admt.202000509

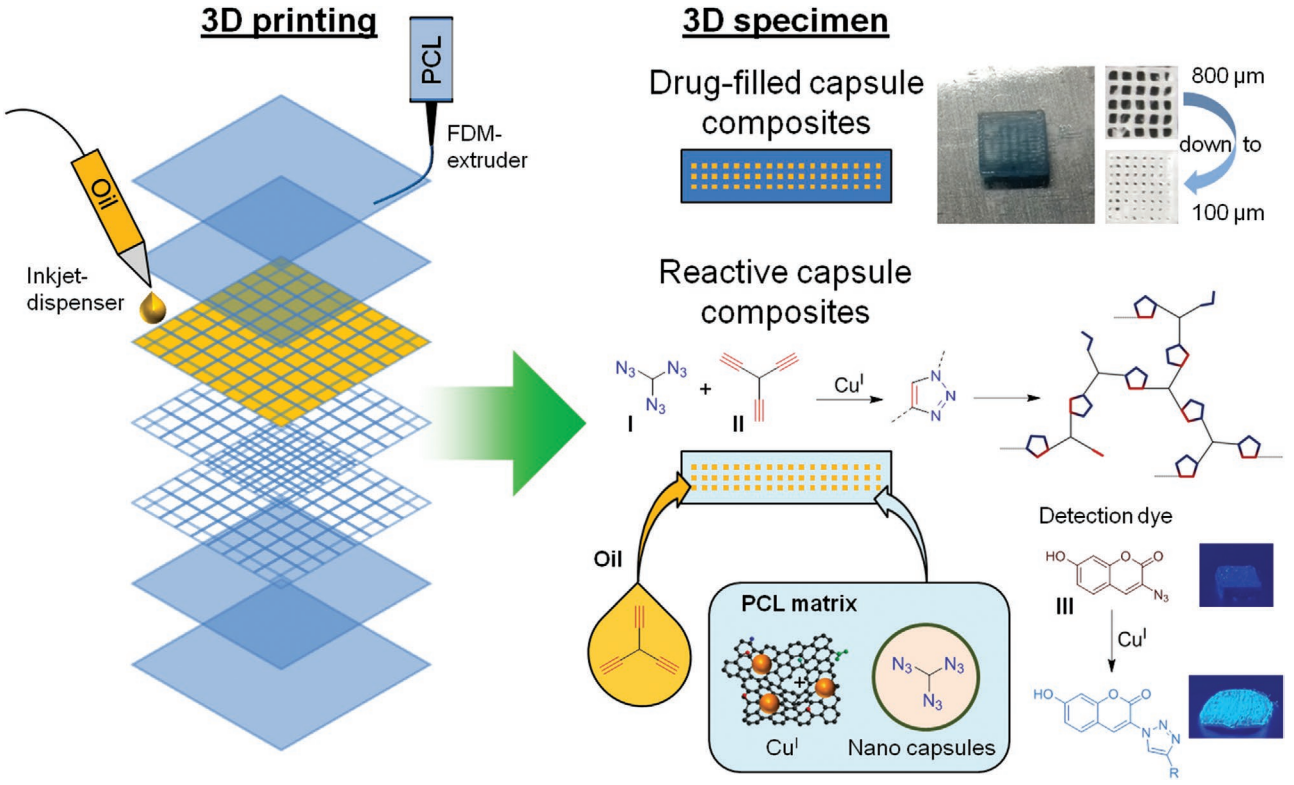

Figure 1. Development of a core–shell capsule system by a two-step printing process. The structure was designed in a CAD program creating fully closed base and top layers with tightly connected polymer strands and an inner grid structure of voids with adjustable size. In the FDM process, the base layer was manufactured first and the polymer grid was deposited on top. Microcapsule-voids were filled with oil by a second printing head and finally closed by the top layer processed with FDM again. The process was adapted to reactive systems of components I and II, able to react in a Cu^{I}-catalyzed "click" reaction after 3D printing. If component III is included additionally, the material reports the "click" reactivity via a fluorogenic dye, generated by the "click" reaction.

arrays, and the ability to control the core volumes, compositions, and shell thicknesses.[15] Recently, solid dosage tablets containing drug-loaded nanocapsules were printed by FDM using PCL filament, placing the freshly printed tablets into a nanocapsules suspension to attach the nanocapsules onto the surface of the printed structures.[16]

This paper reports on a novel method to 3D-print micro-sized capsules into a thermoplastic polymer matrix, by combining different 3D printing techniques and composite printing. The approach aims to generate highly functional composite materials based on multi-compartment structures, mixing a biodegradable polymer (PCL) with nanocapsules and micro scaled fillers, while creating micro-sized capsules during printing and filling them with hydrophobic liquids (**Figure 1**). Void spaces generated during the FDM-process were filled with liquids using a separate liquid dispenser, placed within the same 3D printing system. Based on this method, 3D printing of a known capsule-based self-healing composite, superior over the previous conventional mold casting method, could be realized.[17] The special challenge in using the 3D printing system was the use of two reactive components both embedded into a thermoplastic polymer containing a solid catalyst, which in turn can lead to an externally triggered crosslinking chemistry to enable the design of self-healing materials. In contrast to conventional encapsulation methods, such as in-situ polymerization,[18] interfacial polymerization,[19] sol-gel methods,[20] or solvent-evaporation emulsion,[21] we here use the 3D printing directly to dispense the liquid within a solid matrix during the FDM-printing process.

2. Material Design and Components

3D printing was based on generating a square area of 5 × 5 mm, completely filled with polymer composite, subsequently placing the next layers as a grid structure to form micrometer sized voids with a width of ≈100 to 800 µm. These gaps were filled with a liquid component in a drop-on-demand manner, enclosing the top layer by the FDM-process (Figure 1 and Figure S1, Supporting Information). The base and top structures were designed in a CAD program creating fully closed layers with tightly connected polymer strands. The capsule structure between the base and top layers was programmed as an oil-filled grid system that contained both grid directions (90° rotated) in one layer level (see Figure 3c,d). In the FDM process, the base layer was first manufactured and the polymer grid was deposited on top. The still open microcapsule voids were filled with the liquid oil by a second printing head and finally closed by the top layer, processed with FDM again. These combined 3D printing processes created the opportunity to manufacture drug-filled capsule systems

as well as reactive capsule composites in one single 3D printing cycle. As a final proof of principle, the reactive capsule composites were containing two different liquids for a fluorogenic CuAAC "click" reaction (copper(I)-catalyzed alkyne azide cycloaddition), catalyzed by a heterogeneous catalyst: thermally reduced graphene oxide containing Cu(I)-nanoparticles (later called TRGO).[17a–c]

3. Encapsulation of Hydrophobic Model Liquids

First, the printing of non-reactive liquids, such as farnesol, linalool, limonene, and a reactive trivalent alkyne (II) into structures of pure polycaprolactone (PCL) was tested. The core–shell capsule composite was generated with the help of the regenHU BioCAD software with three different layer styles. Three different molecular weights (14, 45, and 80 kDa) were tested for their temperature depended viscosity to ensure the printability with the regenHU 3DDiscovery (**Figure 2**a). As already demonstrated in a recent publication with this 3D printer, the viscosity range of the polymer extruder is situated in the range of 200–2000 Pa s.[22] Combined with a melting point of around 60 °C for PCL, this allows the use of ≈ 45 kDa molecular weight at a printing temperature of 80–90 °C, whereas both the 80 kDa PCL and the low-molecular-weight PCL (14 kDa) required too high printing temperatures (above 100 °C), or were displaying too low a viscosity for stable printing. Thermal stabilities of all printed liquids were sufficient at around 80 °C (Figure 2b, TGA diagrams, details in **Table 1**).

All model-liquids could be used in this 3D printing process in a temperature range of 40–100 °C, as the contact with the freshly extruded, hot PCL did not lead to evaporation or decomposition of the embedded liquids. The interaction between the hot PCL surface directly after FDM-deposition and the hydrophobic liquid drops played an important role in the 3D printing process (Table S1, Supporting Information), as the liquids were deposited as small droplets (1–5 µL) into the created gaps between the PCL strands and on top of the base-PCL layer. Therefore, wetting between the dispensed liquid and the PCL-polymer is important for proper filling of the voids with the liquids. After the 3D printing of PCL cuboids (5 × 30 × 0.9 mm) the contact angle of the dispensed liquids (limonoene, linaool, farnesol, and the alkyne (II)) were determined as $\gamma \approx 0°$ (Table S1, Supporting Information). This results that the processing under the chosen conditions yielding the final core–shell capsule composites using 3D printing was possible. The liquid oil would fill up all the small irregularities and created capsule voids, thus generating void-free embedded liquid capsules. In contrast, when dispensing pure water it formed a droplet on top of the PCL (Table S1, Supporting Information) and air filled gaps were left between them due to the largely different surface tension.[23] Thus, the dispensing of, for example, aqueous solution would require a different polymer displaying a different surface tension.

For simultaneous printing of two different materials with a large difference in viscosity, the dual head 3D printer regenHU 3DDiscovery was used. The printer was equipped with a heatable polymer printing head that consisted of a storage tank and

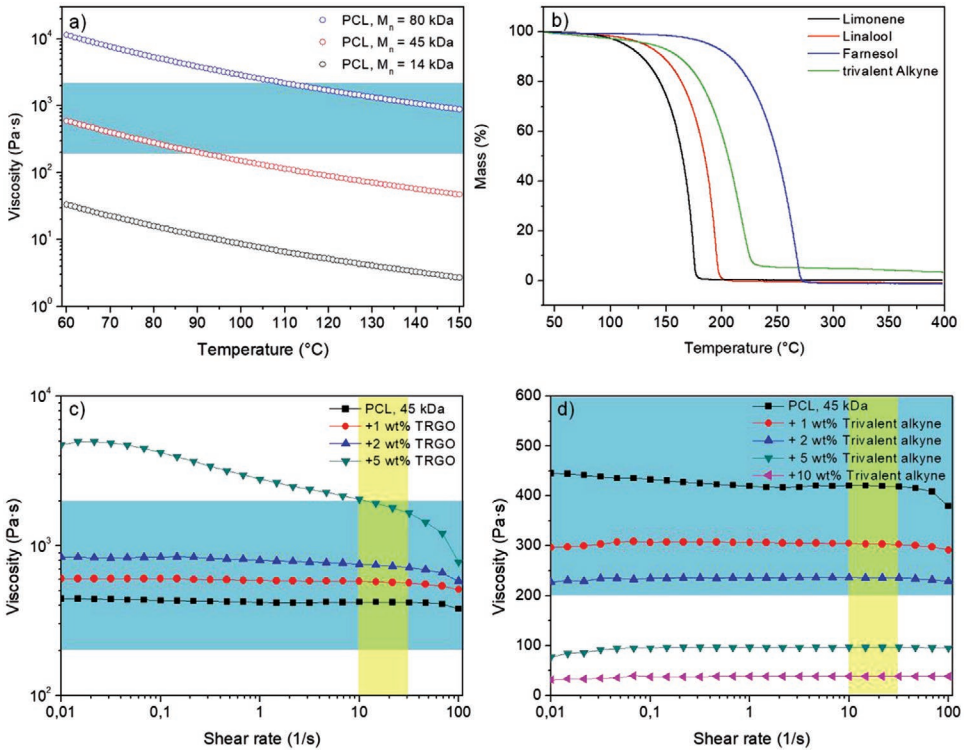

Figure 2. a) Temperature dependent rheology measurements for poly(caprolactone) (PCL) with different molecular weights (M_n = 14, 45, 80 kDa). The printing range of the 3D printer is marked in blue. b) Thermal decomposition measurements of the used hydrophobic oils under an atmosphere of nitrogen with a heating rate of 10 °C min^{-1}. c) Melt-rheology of PCL composites at 80 °C with TRGO and d) the trivalent alkyne (II) to ensure printability with the regenHU 3DDiscovery printer (η = 200–2000 Pa s, γ = 10–30 s^{-1}).

Table 1. Thermal stability and analysis of limonene, linalool, farnesol, and the trivalent alkyne (II).

Liquid	ϑ_{Onset} [°C]	ϑ_{End} [°C]	Mass loss$_{400\ °C}$ [%]
Limonene	102	177	99.9
Linalool	116	197	99.9
Farnesol	178	270	99.9
Triv. alkyne	109	225	97.2

a screw extruder as well as a drop-on-demand inkjet printing head for liquids (Figure S1, Supporting Information). The inkjet head could be used with liquids in the range of 1–10 mPas. The preheated PCL in the storage tank (90 °C) was moved with air pressure of p = 0.20 MPa into the screw extruder and then extruded through a steel nozzle, printing the objects on top of the double-sided adhesive tape. The hydrophobic liquids were then dispensed via a 3 mL syringe, attached onto the drop-on-demand printing head, applying an air pressure of 0.01–0.04 MPa. After printing of the core–shell capsule composites, the sample surfaces were rinsed with ethanol to remove excess liquid and adhesive residues. The process is shown in **Figure 3**a–e, displaying the cleaned PCL-grids.

A critical point in this work was to generate completely closed capsule systems, which contain the hydrophobic oil or a dye for visualization. Tightness of the 3D printed composite was proven by light microscopy and via diffusion tests of fluorescein filled capsules (Figure 3a,b). As shown in Figure 3c, it was possible to 3D print completely closed layers with capsule sizes down to 100 microns, with a maximum size of 800 microns. The single polymer strands were well connected and the turns over points at the end of the specimen were also filled with PCL. Gaps in the range of micrometer or millimeter were not visible. With good development of the design and optimal printing conditions a core–shell capsule matrix could therefore be realized.

To further prove the encapsulation of liquids inside the core–shell capsule, matrix diffusion tests were conducted (see Figure 3g). A saturated solution of fluorescein in farnesol was prepared and used in the above-described printing process. The so prepared specimen was placed in a quartz cell filled with 3 mL ethanol, checking efflux of fluorescein with fluorescence measurements at 519 nm for up to 100 h. The filled capsules started to continuously leach after 10 h into the surrounding ethanol, observing a linear increase of fluorescence intensity, stopping after ≈50 h. Based on the lag phase of ≈10 h and the subsequent slow release, we conclude the formation of very well enclosed capsules.

An advantage of our 3D printing technology is the ability to create capsule-based specimens with the opportunity to steplessly change the size of the capsules (see Figure 3c). The grid arrays defining the capsule size in the final material could be tuned in all 3D directions to gain capsule sizes from 100 to 800 µm. The reprintability of the core–shell capsule composites were analyzed with weight measurements being around 43 mg with a standard deviation below 1 mg (Table S2, Supporting Information).

4. Reactive Capsule Composites

The 3D printing approach was then adapted to a capsule based self-healing composite, consisting of a heterogeneous Cu(I)-catalyst (TRGO), the trivalent azide (I), and the trivalent alkyne (II).[17a–c] The desired composites are based on PCL, containing 10–15 wt% azide(I)-nanocapsules (Figures S2 and S3, Supporting Information) and a corresponding amount of

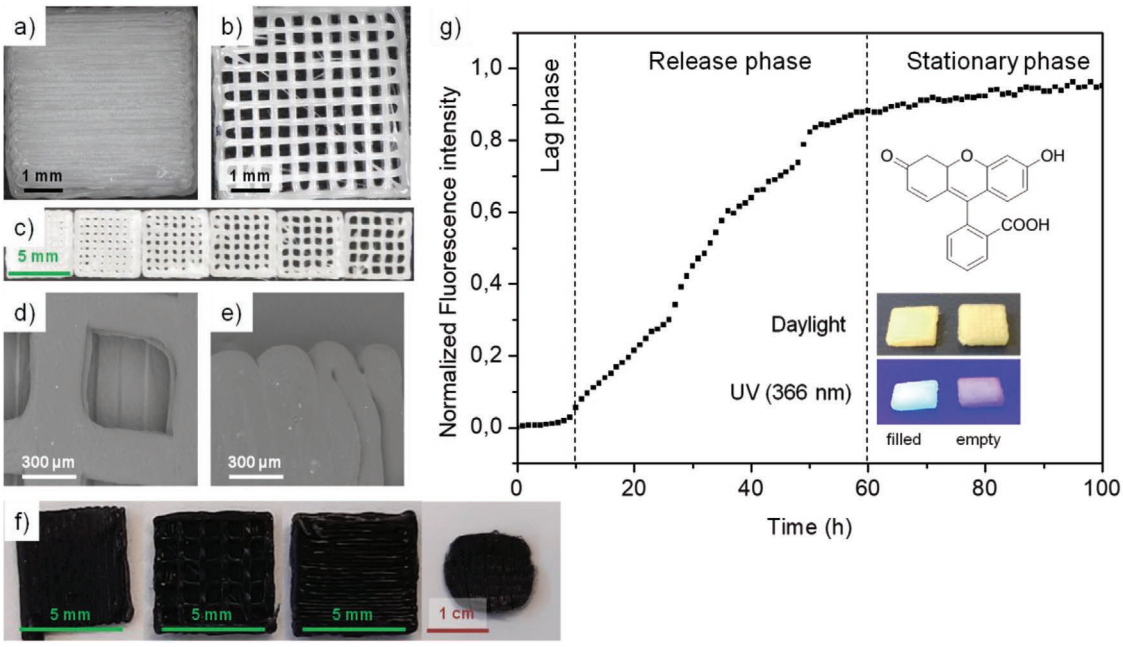

Figure 3. a) Microscopic image of the printed top layer (5 mm × 5 mm) to enclose the core–shell capsule system, b) the inner grid structure forming the capsule system, and c) different grid sizes with gaps from 100 to 800 µm. SEM images of d) one capsule void, e) the top layer, and f) pictures of different layers of the composite 10 during printing as well as a compressed/damaged sample. g) Diffusion test of printed core–shell capsule systems with fluorescein saturated farnesol solution as capsule filling. The release of the solution in ethanol was analyzed by fluorescence measurements.

Table 2. Overview on the core–shell capsule composite components. The composites include poly(ε-caprolactone), PVF-azide(I)-nanocapsules, and the heterogeneous Cu^{I}-catalyst TRGO. The alkyne component II was added with the liquid printing head in a drop-on-demand process. The composites were based on 500 × 500 × 400 micrometer capsule size created by FDM.

Sample	PCL [g]	Capsules [g]	Azide I content in the capsules	TRGO [mg]	Alkyne II [µL]
Composite 10	2	0.2	0.090 g	3	2.5
Composite 10C	2	0.2	0.090 g + 2.34 mg Coumarin	3	2.5
Composite 15	2	0.3	0.135 g	4.5	2.5

TRGO,[17a] able to catalyze a chemical reaction triggered by an external stimulus, as azides and alkynes are known to react in a "CuAAC-click" reaction.[24] Two different trivalent monomers, one bearing azide groups (I), the other bearing alkyne groups (II), were separated by encapsulation methods and could then react after activation via a Cu(I)-catalyzed Huisgen-1,3-dipolar cycloaddition under a formation of 1,4-triazole crosslinked resin.[24,25] We aimed to transform the known mold based fabrication into a 3D-printed-based approach. Since the final composite consisted of the PCL matrix, a graphene-based TRGO catalyst (containing catalytic CuO_2-nanoparticles), the azide(I)-filled nanocapsules (200 nm), and a trivalent, reactive alkyne (II), we first probed changes in melt-viscosity of the PCL melt at 80 °C upon addition of the catalyst in amounts of 1–5 wt% TRGO (Figure 2c). In the range of the shear rates applied during printing, the viscosity of the composite increases from 440 to 4800 Pa s. Considerable shear-thinning behavior was observed, in line with known effects from graphene-sheets in molten polymers, where the carbon layers arrange parallel to the extrusion direction of the filament.[26] Admixing the liquid trivalent alkyne (II) with PCL at 80 °C (Figure 2d), lead to a decrease of the viscosity from 440 to 32 Pa s. There was no significant shear rate dependency due to the solvent like behavior of trivalent alkyne (II) within the PCL. Based on the printing range of the 3D printer,[22] PCL with up to 5% TRGO content and a trivalent alkyne II content of up to 2% was identified as printable.

The prepared composites 10, 10C, and 15 containing PCL mixed with TRGO and PVF-azide nanocapsules (**Table 2**) were placed into the FDM printing head at a temperature of 85–90 °C. The use of poly(vinyl formal), PVF (T_g = 105 °C), as shell material is crucial to maintain a stable capsule shell at the extrusion temperature. At the printing nozzle (ID = 330 µm) the composites were extruded at 75–80 °C. The second reaction component, the trivalent alkyne (II), was placed into the second liquid inkjet print head.

A composite structure with a square base shaped 5 × 5 mm and a grid with gaps of around 500 µm were designed in the BioCAD program. First, two layers of a completely filled base area were printed. Subsequently, 2–3 layers of the grid structure, forming the 3D printed capsules, were printed on top. In between the second printing head with the liquid drop on demand function dispensed the trivalent alkyne (II) into the created gaps, filling them with a volume of ≈6 nL to ≈380 nL per capsule void. As a final closing layer two completely filled composite layers were printed again on top. In Figure 3e,f, each step was stopped separately to obtain images and SEM images. A good closure of the 3D printed capsules could be achieved, also showing uniform extrusion in the SEM pictures and the formation of rectangular capsules, later filled with the trivalent alkyne (II). The SEM image (Figure 3d) clearly showed that both grid strands (90° rotated strands) were in one layer level forming separated microcapsules.

The thermal stability of the composites, the azide (I), and the catalyst were analyzed with thermogravimetric analysis (**Figure 4**) under nitrogen and a heating rate of 10 °C min^{-1}. The reactive trivalent azide (I) was stable up to 200 °C and decomposed in a temperature range of 200–400 °C leading to a composite mixture stable in the temperature range of FDM printing (75–90 °C). In the range of 250–400 °C a small mass loss of 7.4% or 9.7% occurred, which could be related to the decomposition of the azide filling. The matrix polymer PCL and the capsule shell material PVF decomposed at temperatures of 400–450 °C, indicating that no thermal induced decomposition reactions took place during printing of the composites.

We subsequently tested for the residual reactivity of the embedded components, both able to react via "click" reactions, catalyzed by the TRGO-catalyst via the embedded CuO_2-nanoparticles. Reaction tests for the post-printing reactivity (possible self-healing application) were accomplished by calorimetry via DSC to check for the reaction enthalpy of the embedded healing components and the TRGO catalyst after printing, calibrated to the enthalpy of the "click" reaction for one triazole ring.[17b,c] We tested the reactivity of all components directly after printing (**Table 3**, entries 3 and 6 and second-run DSC entry 4 and 7) and after heating to a temperature of 40 °C for 3 days, where the "click" reaction has already taken place, but PCL remains structurally stable (entries 5 and 8).

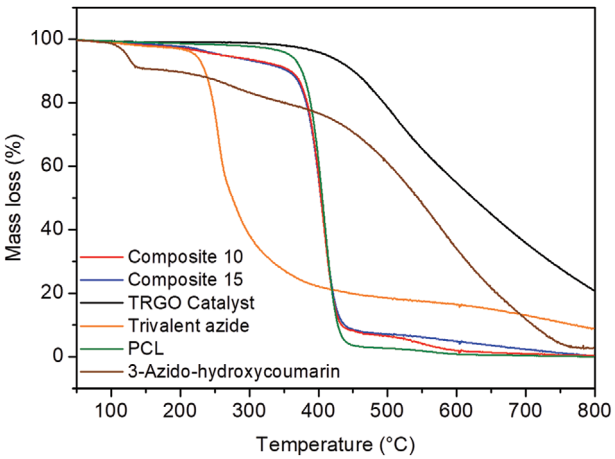

Figure 4. Thermal decomposition measurement of the composite mixtures (10, 15 wt%), TRGO catalyst, PCL, and the trivalent azide (I) under nitrogen atmosphere with a heating rate of 10 °C min^{-1}.

Table 3. DSC analysis of the reactive "click" mixture after printing and compression as well as of the samples after self-healing test for 3 days at 40 °C.

Entry	Reaction	ϑ_{Onset} [°C]	ϑ_{Peak} [°C]	ΔH_R [J·mol^{-1}]	Conversion [%]
1	Thermal click reaction of pure I and II	86.5	140.8	–124.10	47
2	Click reaction of pure I and II with TRGO	58.1	72.1	–86.78	33
3	Composite 10 directly after printing	79.8	104.4	–0.82	7
4	Composite 10 (second run)	–	–	–	0
5	Composite 10 (40 °C, 3 days)	–	–	–	0
6	Composite 15 directly after printing	84.7	103.1	–3.91	22
7	Composite 15 (second run)	–	–	–	0
8	Composite 15 (40 °C, 3 days)	–	–	–	0

The ruptured nano- and microcapsules (after applying a compression force) released their liquid fillings (I, II), which then mix and react in the Cu(I)-catalyzed "click" reaction. One sample of each composite was analyzed directly after printing via DSC (Table 3, **Figure 5**). In the composites (entry 3 and 6 and second-run DSC in entry 4 and 7), the trivalent monomers reached conversions of 7% (composite 10) and 22% (composite 15), concluding that the two "click" components (I) and (II) were still active after the printing process, concluding that the PVF-shells have been at least partially retained. The purely thermal, non-catalyzed reaction showed an overall conversion of around 47% (Table 3, entry 1 and Figure S6, Supporting Information), the reaction with the heterogeneous TRGO catalyst lead to a conversion of 33% (Table 3, entry 2 and Figure S6, Supporting Information). As expected, the second DSC run for all samples (entry 7 and entry 7) did not show a "click" reaction after the melting of PCL as both reaction components I and II have then already reacted. After treating the printed samples of the same composites at 40 °C for 3 days (after capsule rupturing)[17a–c] (Table 3, entries 5 and 8, Figure 5) indicating that under these conditions the "click" reaction has already taken place. The DSC measurements and reaction heat analysis proved our concept of reactive component encapsulation with a multi-material 3D printing, still being active after printing and able to react partially below the melting point of PCL.

The reactivity of the core–shell capsule composites could be quantified further with the inclusion of a fluorogenic dye for stress- or damage detection, where an embedded fluorogenic dye showed a strongly increased intensity after the "click" reaction.[27] PVF-azide(I)-filled nanocapsules were modified

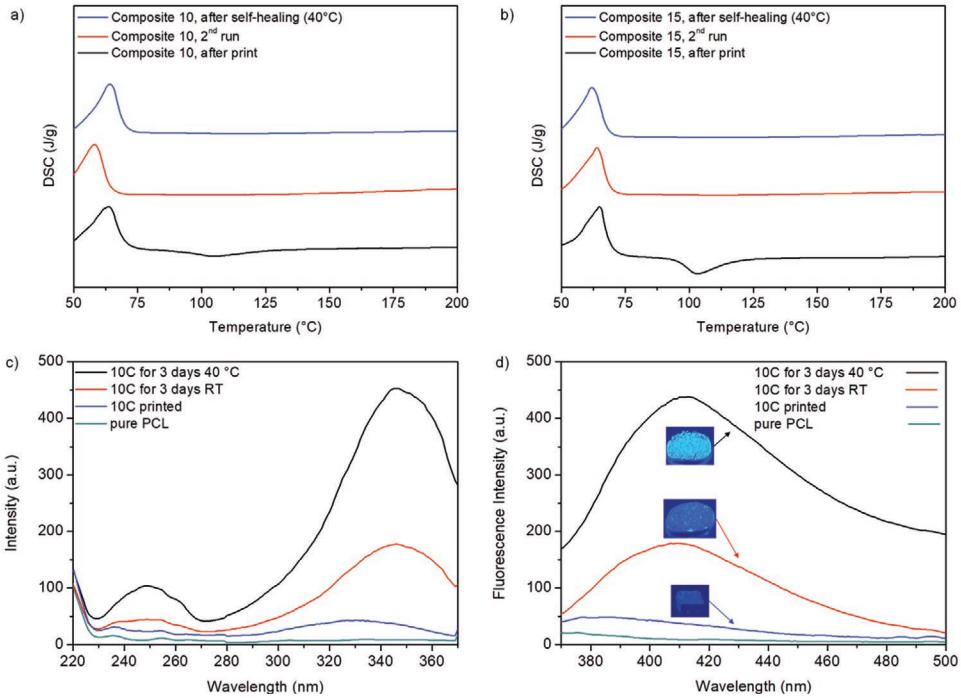

Figure 5. DSC analysis of the "click-based" reaction between trivalent azide (I) and the trivalent alkyne (II). The freshly printed and ruptured composites (—) show a reaction peak after the melting of point of PCL: a) composite 10 and b) composite 15. In the second run of these samples (—) no reaction is observed. When the samples are treated at 40 °C for 3 days (—) there is also no reaction peak, concluding the reaction already occurred. c) Fluorescence excitation and d) emission measurements of solid composite 10C samples after the different stages of the "click" reaction as well as images of the composite 10C in UV light (366 nm).

with 1.5 wt% of 3-azido-hydroxycoumarin (III) leading to yield *composite 10C*. After calibration and evaluation of the dye content inside the capsules (Figure S7 and Table S5, Supporting Information), composite 10C was printed adding the fluorogenic dye (III) in the same way as in the composites 10, 15. After damaging the samples (applying compression force) the increase of fluorescence intensity of the dye, generated by the fluorogenic "click" reaction was measured. A significant change in fluorescence intensity could be measured by solid state fluorescence measurements in the reflection mode and visualized by a UV-lamp at 366 nm (Figure 5c,d). Pure PCL and the freshly printed composite 10C were showing only a neglectable fluorescence at 410 nm. Increased fluorescence intensity, compared to the virgin composite 10C, was observed for the samples stored for 3 days at room temperature and 40 °C. Therefore, the "click" reaction between the trivalent alkyne (II), dispensed by the second printing head, and the 3-azido-hydroxycoumarin (III) can be used for damage detection as well as reaction control. This proves the concept of successful core–shell capsule printing. The possibility to perform a "click" reaction at temperature around 40 °C opens the field for self-healing capsule-based-composites without destroying the created and printed structures.

5. Conclusion

A novel 3D printing process is reported, where a dual-dispensing system allows printing liquid-filled capsules into a solid, thermoplastic matrix. Our approach enables to generate functional composite materials based on multi-compartment structures, with a biodegradable polymer (PCL) filled with premixed nanocapsules and micro scaled liquid-filled capsules. Voids generated during the printing process are filled with various hydrophobic liquids, ranging from simple farnesol, limonene, to trivalent a azide, useful for a subsequent capsule based, self-healing material. Capsules with sizes down to 100 micron and up to 800 microns can be printed reliably. It was demonstrated that the two reactive components can be efficiently separated via closed capsules, directly embedded into the PCL-polymer. Thermal stability of the printing process allows retaining sufficient reactivity for a subsequent "click" reaction, underscoring the possibility to embed two separate, highly reactive components into one and the same thermoplastic material. This approach was used for a proof-of-concept self-healing material, based on capsules and a triggered "click" reaction, visualized by a fluorogenic dye. With the here developed methodology, a large variety of multicomponent materials can now be addressed, allowing to choose the components, their embedding into multicomponent materials and the final morphology in a highly flexible manner. Based on this method, we can 3D-print multicomponent materials as an advanced method over the conventional mold casting methods. There is a great chance to apply this type of printing in electrochemical devices (e.g., electrodes, ionogels), in the generation of complex microfluidic systems, as well as in the generation of novel solar cell-systems, where thin films are directly printed into multilayered structures. Additionally, pharmaceutically release-materials can now be printed, tuning the release of capsule-embedded drugs via the controllable thickness of the surrounding polymer. The comparable adjustment of many different components avoids the need for individual rheological adjustment for each ink-composition, thus hoping to open a bright range of application in material science.

6. Experimental Section

For 3D printing, the pure poly(ε-caprolactone) granulate (M_n = 45 kDa, Sigma-Aldrich) was placed into the storage tank of the polymer extrusion head. In a same manner were the capsule-based composites 10, 10C, and 15 used. They were prepared by mixing TRGO (3–5 mg, 20 µm flakes) and PVF-azide(I) capsules (200–300 mg, 200 nm) into molten PCL (2 g) at 80 °C. The complex geometrical shapes were programmed with the help of the CAD program BioCAD. Each polymer strand was drawn inside the CAD-program and the liquid filling was programmed in a drop-on-demand manner. For the attached 0.2/0.33 mm printing nozzle the strand thickness was set to 90% of the nozzle. The CAD-file was saved, transformed to an ISO file and sent to the 3D printer. The printer regenHU 3DDiscovery, equipped with a heatable polymer extrusion printing head with a metal nozzle, was used for printing of polymer composites. Each composite was filled into the heatable tank of the printing head (80–90 °C). The temperature of the printing nozzle was adjusted to 70–80 °C according to the rheology data. The temperature of the tank of the printing head was set 10 °C higher than the temperature of the printing nozzle. Pressured air of 0.20 MPa was used to transport the molten composite inside the printing head. The composites were printed on a standard glass slide equipped with masking tape for mechanical adhesion. The drop-on-demand liquid printing head was set to one drop per grid hole at room temperature. The 3 mL cartridge was filled with oils and pressed with air of 0.01–0.04 MPa to move the liquid through the inkjet nozzle, for example, farnesol, trivalent alkyne (II).

For rheology measurements, the polymer and the composites samples were mixed in DCM and dried in vacuum at 60 °C for 3 days. On an Anton Paar MCR-101 DSO rheometer the rheology measurements were accomplished using parallel plate-plate geometry with a diameter of 8 mm. The temperature was controlled with a thermoelectric cooler/heater in a chamber filled with dry air. For each measured temperature, the samples were preheated for 20 min reaching their equilibrium state. Temperature-dependent measurements of the viscosity versus shear rate (0.1–100 s^{-1}) were performed to get 3D printing information. The measured data were analyzed by using the RheoPlus/32 software (V 3.40) and OriginPro8G.

Contact angle measurements were performed on an Optical Contact Angle Measuring System OCA 20. Three drops of each liquid were placed onto the surface of the printed PCL plates (1 drop 5 µL). The contact angle was determined on both sides of the drop using OCA 20 instrument at a temperature of 20 °C.

Supporting Information

Supporting Information is available from the Wiley Online Library or from the author.

Acknowledgements

The authors thank the Leistungszentrum "System- und Biotechnologie" (Uni-CBS1) for financial support as well as DFG SFB TRP 102/TP A03, DFG BI 1337/14-1 and BAT4EVER project founded by the European Union in the scope of H2020-LC-BAT-2020-3.

Open access funding enabled and organized by Projekt DEAL.

Conflict of Interest

The authors declare no conflict of interest.

Keywords

3D printing, click reaction, core–shell capsules, drug delivery, stress detection

Received: May 25, 2020
Revised: June 25, 2020
Published online: September 21, 2020

[1] a) S. B. Kamaljit, R. Singh, H. Singh, *Rapid Prototyping J.* **2016**, *22*, 281; b) O. A. Mohamed, S. H. Masood, J. L. Bhowmik, *Adv. Manuf.* **2015**, *3*, 42; c) S. Crump, in *ASME Annual Winter Conf.*, Vol. *50*, ASME, New York **1991**, pp. 53–60; d) S. Crump, in *Proc. 2nd Int. Conf. on Rapid Prototyping*, **1991**, pp. 358–361.

[2] X. Wang, M. Jiang, Z. Zhou, J. Gou, D. Hui, *Composites, Part B* **2017**, *110*, 442.

[3] a) D. T. Nguyen, T. D. Yee, N. A. Dudukovic, K. Sasan, A. W. Jaycox, A. M. Golobic, E. B. Duoss, R. Dylla-Spears, *Adv. Mater. Technol.* **2019**, *4*, 1900784; b) G. Weisgrab, A. Ovsianikov, P. F. Costa, *Adv. Mater. Technol.* **2019**, *4*, 1900275.

[4] J. Wong, A. T. Gong, P. A. Defnet, L. Meabe, B. Beauchamp, R. M. Sweet, H. Sardon, C. L. Cobb, A. Nelson, *Adv. Mater. Technol.* **2019**, *4*, 1900452.

[5] Z. Ji, C. Yan, B. Yu, X. Zhang, M. Cai, X. Jia, X. Wang, F. Zhou, *Adv. Mater. Technol.* **2019**, *4*, 1800713.

[6] J. Lim, Y. K. Kim, D.-J. Won, I. H. Choi, S. Lee, J. Kim, *Adv. Mater. Technol.* **2019**, *4*, 1900118.

[7] a) Y. Cao, X. Zhu, H. Chen, X. Zhang, J. Zhou, Z. Hu, J. Pang, *Sol. Energy Mater. Sol. Cells* **2019**, *200*, 109945; b) Y. Cao, X. Zhu, J. Jiang, C. Liu, J. Zhou, J. Ni, J. Zhang, J. Pang, *Sol. Energy Mater. Sol. Cells* **2020**, *206*, 110279; c) W. Liu, J.-j. He, Z.-g. Li, W.-l. Jiang, J.-b. Pang, Y. Zhang, Y. Sun, *Phys. Scr.* **2012**, *85*, 055806; d) Y. Zhou, Y. Huang, J. Pang, K. Wang, *J. Power Sources* **2019**, *440*, 227149.

[8] a) C. I. Gioumouxouzis, O. L. Katsamenis, N. Bouropoulos, D. G. Fatouros, *J. Drug Delivery Sci. Technol.* **2017**, *40*, 164; b) C. I. Gioumouxouzis, A. Baklavaridis, O. L. Katsamenis, C. K. Markopoulou, N. Bouropoulos, D. Tzetzis, D. G. Fatouros, *Eur. J. Pharm. Sci.* **2018**, *120*, 40; c) S. A. Khaled, J. C. Burley, M. R. Alexander, J. Yang, C. J. Roberts, *J. Controlled Release* **2015**, *217*, 308; d) Y.-F. Zhang, C. J.-X. Ng, Z. Chen, W. Zhang, S. Panjwani, K. Kowsari, H. Y. Yang, Q. Ge, *Adv. Mater. Technol.* **2019**, *4*, 1900427.

[9] D. Markl, J. A. Zeitler, C. Rasch, M. H. Michaelsen, A. Müllertz, J. Rantanen, T. Rades, J. Bøtker, *Pharm. Res.* **2017**, *34*, 1037.

[10] a) A. Melocchi, F. Parietti, G. Loreti, A. Maroni, A. Gazzaniga, L. Zema, *J. Drug Delivery Sci. Technol.* **2015**, *30*, 360; b) A. Maroni, A. Melocchi, F. Parietti, A. Foppoli, L. Zema, A. Gazzaniga, *J. Controlled Release* **2017**, *268*, 10; c) A. Melocchi, F. Parietti, S. Maccagnan, M. A. Ortenzi, S. Antenucci, F. Briatico-Vangosa, A. Maroni, A. Gazzaniga, L. Zema, *AAPS PharmSciTech* **2018**, *19*, 3343; d) C. Nober, G. Manini, E. Carlier, J.-M. Raquez, S. Benali, P. Dubois, K. Amighi, J. Goole, *Int. J. Pharm.* **2019**, *569*, 118581.

[11] T. C. Okwuosa, C. Soares, V. Gollwitzer, R. Habashy, P. Timmins, M. A. Alhnan, *Eur. J. Pharm. Sci.* **2018**, *118*, 134.

[12] a) A. Goyanes, J. Wang, A. Buanz, R. Martínez-Pacheco, R. Telford, S. Gaisford, A. W. Basit, *Mol. Pharmaceutics* **2015**, *12*, 4077; b) S. A. Khaled, J. C. Burley, M. R. Alexander, J. Yang, C. J. Roberts, *Int. J. Pharm.* **2015**, *494*, 643; c) D. Smith, Y. Kapoor, A. Hermans, R. Nofsinger, F. Kesisoglou, T. P. Gustafson, A. Procopio, *Int. J. Pharm.* **2018**, *550*, 418; d) G. K. Eleftheriadis, C. S. Katsiotis, N. Bouropoulos, S. Koutsopoulos, D. G. Fatouros, *Pharm. Dev. Technol.* **2020**, *25*, 517; e) T. C. Okwuosa, B. C. Pereira, B. Arafat, M. Cieszynska, A. Isreb, M. A. Alhnan, *Pharm. Res.* **2017**, *34*, 427.

[13] D. Chen, X.-Y. Xu, R. Li, G.-A. Zang, Y. Zhang, M.-R. Wang, M.-F. Xiong, J.-R. Xu, T. Wang, H. Fu, Q. Hu, B. Wu, G.-R. Yan, T.-Y. Fan, *AAPS PharmSciTech* **2020**, *21*, 6.

[14] a) S. Ilkhanizadeh, A. I. Teixeira, O. Hermanson, *Biomaterials* **2007**, *28*, 3936; b) E. D. F. Ker, B. Chu, J. A. Phillippi, B. Gharaibeh, J. Huard, L. E. Weiss, P. G. Campbell, *Biomaterials* **2011**, *32*, 3413; c) E. D. F. Ker, A. S. Nain, L. E. Weiss, J. Wang, J. Suhan, C. H. Amon, P. G. Campbell, *Biomaterials* **2011**, *32*, 8097; d) E. D. Miller, K. Li, T. Kanade, L. E. Weiss, L. M. Walker, P. G. Campbell, *Biomaterials* **2011**, *32*, 2775.

[15] M. K. Gupta, F. Meng, B. N. Johnson, Y. L. Kong, L. Tian, Y.-W. Yeh, N. Masters, S. Singamaneni, M. C. McAlpine, *Nano Lett.* **2015**, *15*, 5321.

[16] R. C. R. Beck, P. S. Chaves, A. Goyanes, B. Vukosavljevic, A. Buanz, M. Windbergs, A. W. Basit, S. Gaisford, *Int. J. Pharm.* **2017**, *528*, 268.

[17] a) S. Rana, D. Döhler, A. S. Nia, M. Nasir, M. Beiner, W. H. Binder, *Macromol. Rapid Commun.* **2016**, *37*, 1715; b) A. Shaygan Nia, S. Rana, D. Döhler, X. Noirfalise, A. Belfiore, W. H. Binder, *Chem. Commun.* **2014**, *50*, 15374; c) A. Shaygan Nia, S. Rana, D. Döhler, W. Osim, W. H. Binder, *Polymer* **2015**, *79*, 21; d) N. Kargarfard, N. Diedrich, H. Rupp, D. Döhler, W. H. Binder, *Polymers* **2018**, *10*, 17.

[18] E. N. Brown, M. R. Kessler, N. R. Sottos, S. R. White, *J. Microencapsulation* **2003**, *20*, 719.

[19] R. Arshady, *J. Microencapsulation* **1989**, *6*, 13.

[20] H. Zhang, X. Wang, D. Wu, *J. Colloid Interface Sci.* **2010**, *343*, 246.

[21] a) Y. Zhao, J. Fickert, K. Landfester, D. Crespy, *Small* **2012**, *8*, 2954; b) Y. Zhao, D. Döhler, L.-P. Lv, W. H. Binder, K. Landfester, D. Crespy, *Macromol. Chem. Phys.* **2014**, *215*, 198.

[22] H. Rupp, D. Döhler, P. Hilgeroth, N. Mahmood, M. Beiner, W. H. Binder, *Macromol. Rapid Commun.* **2019**, *40*, 1900467.

[23] a) L. Averous, L. Moro, P. Dole, C. Fringant, *Polymer* **2000**, *41*, 4157; b) A. Davoudinejad, Y. Cai, D. B. Pedersen, X. Luo, G. Tosello, *Mater. Des.* **2019**, *176*, 107839.

[24] S. Neumann, M. Biewend, S. Rana, W. H. Binder, *Macromol. Rapid Commun.* **2020**, *41*, 1900359.

[25] a) T. V. Hansen, P. Wu, W. D. Sharpless, J. G. Lindberg, *J. Chem. Educ.* **2005**, *82*, 1833; b) M. Meldal, C. W. Tornøe, *Chem. Rev.* **2008**, *108*, 2952; c) L. Zhang, X. Chen, P. Xue, H. H. Y. Sun, I. D. Williams, K. B. Sharpless, V. V. Fokin, G. Jia, *J. Am. Chem. Soc.* **2005**, *127*, 15998.

[26] B. G. Compton, J. A. Lewis, *Adv. Mater.* **2014**, *26*, 5930.

[27] a) Z. Zhou, C. J. Fahrni, *J. Am. Chem. Soc.* **2004**, *126*, 8862; b) C. Le Droumaguet, C. Wang, Q. Wang, *Chem. Soc. Rev.* **2010**, *39*, 1233; c) D. Döhler, S. Rana, H. Rupp, H. Bergmann, S. Behzadi, D. Crespy, W. H. Binder, *Chem. Commun.* **2016**, *52*, 11076.